

See discussions, stats, and author profiles for this publication at: <https://www.researchgate.net/publication/224640406>

Low-order modeling of vehicle roll dynamics

Conference Paper in Proceedings of the American Control Conference · July 2006

DOI: 10.1109/ACC.2006.1657345 · Source: IEEE Xplore

CITATIONS

12

READS

1,764

4 authors, including:



Sean N Brennan

Pennsylvania State University

138 PUBLICATIONS 1,323 CITATIONS

SEE PROFILE

Some of the authors of this publication are also working on these related projects:



Graduate Semi-Autonomous Wheelchair Research [View project](#)



Model-based Prediction of Epileptic Seizures [View project](#)

Low-Order Modeling of Vehicle Roll Dynamics

Bridget C. Hamblin, Ryan D. Martini, John T. Cameron, and Sean N. Brennan, *Member, IEEE*

Abstract— This work presents results of an ongoing investigation into models and control strategies suitable to prevent vehicle rollover due to untripped driving maneuvers. For use as a design model for controller synthesis, low-order models are sought that have sufficient complexity to characterize a vehicle’s roll behavior, yet are not unnecessarily complex or nonlinear. To compare different low-order models found in literature, this work investigates the validity of several roll dynamic models by comparing model prediction to experiment in both the time and frequency domains. Discussion is also given on methods for parametric fitting of the models and areas where significant model error is observed.

Index Terms—Vehicle rollover, vehicle dynamics, modeling of dynamic systems

I. INTRODUCTION

Accidental death due to motor vehicle accidents claim over 1.2 million life-years of un-lived life each year, and is the largest premature death factor for those under the age of 65 [1]. Vehicle accidents are the single largest cause of fatalities for males 44 years and under and for females 34 years and under [2]. These deaths are sudden, and often strike when a person is at the peak of both their professional and personal/family life.

Among the myriad causes of vehicle accidents, rollover stands out as an area deserving of particular focus. While vehicle rollover is involved in only 2.5% of the 11 million accidents a year, it accounts for approximately 20% of all fatalities [3].

To study rollover, the National Highway Traffic Safety Administration (NHTSA) has developed a number of transient maneuvers that are observed to induce untripped wheel lift or even untripped vehicle rollover in some vehicle models [4, 5]. While this experimental approach is unarguably valid for illustrating shortcomings in vehicle behavior, the method does have shortcomings. In particular, it is difficult to definitively establish from only a very small subset of tests whether or not roll safety is ensured over all possible transient maneuvers. Additionally, experimental

results do not directly translate into a vehicle model suitable for rollover mitigation through feedback control. Both factors highly motivate the development of vehicle roll models.

In considering the choice of which roll dynamic model to use, the choice of complexity in the model should match well with the intended use of the model. This study is focused on finding dynamic models that are well suited to the design and implementation of online, real-time controllers to prevent the onset of rollover. A goal of this work and particular departure from previous studies is to not only understand and validate the linear vehicle dynamics of roll behavior, but also to understand the relative impact of various assumptions in creating the vehicle models to ensure the use of the simplest model possible in later controller synthesis.

The remainder of the paper is organized as follows: Section 2 presents preliminaries on nomenclature and model formulation. Section 3 presents several models that will be compared in this study. Section 4 discusses how the inertial parameters of the models were obtained. Section 5 discusses experimental fitting of linear tire parameters. Section 6 details modifications to the linear tire to account for camber. Section 7 presents dynamic model fits. Conclusions summarize the main points.

II. PRELIMINARIES

The following notation is used for each of the models described in this work:

U	Longitudinal velocity (body-fixed frame)
m, m_s	Vehicle mass and sprung mass respectively
I_{xx}, I_{yy}, I_{zz}	Inertia about roll (X), pitch (Y), vertical (Z) axis
I_{xz}	Inertia product
l_f, l_r	Front- and Rear-axle-to-CG distances
L	Track of vehicle ($l_f + l_r$)
K_ϕ	Effective roll stiffness of the suspension
D_ϕ	Effective roll damping of the suspension
h	height from roll axis to CG
α_f, α_r	Slip angle of the front, rear tires
β	Slip angle of the vehicle body
C_f, C_r	Front, Rear cornering stiffness
δ_f	Front steering angle

For ease of comparison model to model, each of the models is presented in a compact symbolic notation of the form:

B. Hamblin and R. Martini are current graduate students at Penn State.
J. T. Cameron is a recent graduate from Mechanical and Nuclear Engineering who is now working with Harris Corp. in Florida.
S. Brennan is an Assistant Professor in the Mechanical & Nuclear Engineering Department, Penn State University, 318 Leonhard Building, University Park, PA 16802. He shares a joint appointment with the Pennsylvania Transportation Institute. (corresponding author, phone (814)863-2430; sbrennan@psu.edu)

$$M \cdot \ddot{q} + D \cdot \dot{q} + K \cdot q = F \cdot u_i \quad (1)$$

where i denotes the model number (1 to 4 for this study), and

$$q = \{y \quad \psi \quad \phi\}^T \quad (2)$$

which denotes the lateral position, yaw angle, and roll angle respectively. The input to the model,

$$u = \{F_f \quad F_r\}^T \quad (3)$$

denotes the front and rear lateral tire forces respectively. The general MDK form described by Eq. (1) allows for an intuitive term-by-term comparison between different models. Further, this MDK form can be readily transformed to the general state-space form of:

$$\frac{dx}{dt} = A \cdot x + B \cdot u \quad (4)$$

with the state vector,

$$x = [V \quad r \quad \phi \quad \dot{\phi}] \quad (5)$$

representing lateral velocity, yaw rate, roll angle and roll rate respectively. The transformation from MDK form to state space is given by the following. Let:

$$R = \begin{bmatrix} 1 & 0 & 0 \\ 0 & 1 & 0 \\ 0 & 0 & 0 \\ 0 & 0 & 1 \end{bmatrix}, \quad S = \begin{bmatrix} 0 & 0 & 0 \\ 0 & 0 & 0 \\ 0 & 0 & 1 \\ 0 & 0 & 0 \end{bmatrix}, \quad T = \begin{bmatrix} 0 & 0 & 0 & 0 \\ 0 & 0 & 0 & 0 \\ 0 & 0 & 0 & 1 \\ 0 & 0 & 0 & 0 \end{bmatrix} \quad (6)$$

and define,

$$E = R \cdot (M - I_3) \cdot R^T + I_4 \quad (7)$$

where I_n represents the identity matrix of size n . Then the state-space matrices A and B are obtained from matrices M , D , K and F as:

$$A = E^{-1} \cdot (-R \cdot D \cdot R^T - R \cdot K \cdot S^T + T) \quad (8)$$

$$B = E^{-1} \cdot (R \cdot F)$$

The state-space form more conveniently allows numerical simulation and model comparisons used in later sections.

III. VEHICLE MODELS

A search of recent literature found over two dozen unique vehicle models inclusive of roll dynamics, but of these, only a few are chosen for further analysis. Considerations used to eliminate certain models are detailed in previous work (see [6]), but the main criteria are based primarily on model complexity, whether or not the model had been validated experimentally by the authors of the model, and how easily model parameters can be measured or inferred.

To emphasize the similarity between the models used in this study, each is presented in the same coordinate system regardless of the coordinate system used in the original publication of the model [7-9]. Herein they all follow the SAE right-handed sign convention shown in Fig 1.

For brevity, details of each model derivation have been omitted from this work, but further details can be found in the original publications [7-9] and in previous work [6]. A discussion of the notable similarities and differences

between the different models can be found in [6].

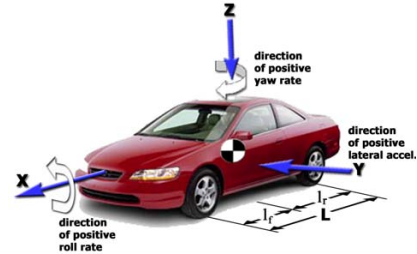


Figure 1: SAE Coordinate System

A. Model 1 - 3DOF Model Assuming Existence of Sprung Mass and No X-Z Planar Symmetry

The most complex model considered in this work is derived by assuming a sprung and unsprung mass, and assuming the unsprung mass has a non-symmetric mass distribution about the x-z plane. It is motivated by the model presented by Mammari et. al. [10]; further details and assumptions are listed therein. Following the MDK form specified earlier, the MDK matrices are given by:

$$M_1 = \begin{bmatrix} m & 0 & m_s h \\ 0 & I_{zz} & -I_{xz} \\ m_s h & -I_{xz} & I_{xx} + m_s h^2 \end{bmatrix} \quad (9)$$

$$D_1 = \begin{bmatrix} 0 & mU & 0 \\ 0 & 0 & 0 \\ 0 & m_s hU & D_\phi \end{bmatrix} \quad (10)$$

$$K_1 = \begin{bmatrix} 0 & 0 & 0 \\ 0 & 0 & 0 \\ 0 & 0 & K_\phi - m_s gh \end{bmatrix} \quad (11)$$

$$F_1 = \begin{bmatrix} 1 & 1 \\ a & -b \\ 0 & 0 \end{bmatrix} \quad (12)$$

B. Model 2 - 3DOF Model Assuming Existence of Sprung Mass and X-Z Planar Symmetry

A common assumption in the above model is that the vehicle is symmetric about the x-z plane, thus making I_{xz} zero and eliminating all cross terms. An example of this is presented by Kim and Park in [8]. In presenting this model, some authors absorb the suspended mass term, mgh , in the (3, 3) element of the K matrix, into the roll stiffness. For example, Kim and Park cited above make this assumption. Placing the equations of motion into the form specified by Eq. (1), the damping, stiffness, and force matrices remain the same,

$$D_2 = D_1, K_2 = K_1, F_2 = F_1 \quad (13)$$

while the mass matrix becomes:

$$M_2 = \begin{bmatrix} m & 0 & m_s h \\ 0 & I_{zz} & 0 \\ m_s h & 0 & I_{xx} + m_s h^2 \end{bmatrix} \quad (14)$$

With the assumption of a symmetric mass distribution, the yaw dynamics are not directly coupled to the roll and sideslip dynamics in the MDK form. In state-space, they can only be coupled through the inversion of the mass matrix, E^{-1} , and through the tire forces, if these forces are dependent on roll.

C. Model 3 - 3DOF Model Assuming Sprung Mass Only

In addition to the assumptions given previously, it is sometimes assumed that the entire mass of the vehicle is concentrated at the sprung mass. The paper by Carlson et. al [7] uses this assumption. To modify previous models to express this assumption, the unsprung mass is made zero and the sprung mass is made equal to the total mass of the vehicle. The resulting MDK matrices are:

$$M_3 = \begin{bmatrix} m_s & 0 & m_s h \\ 0 & I_{zz} & 0 \\ m_s h & 0 & I_{xx} + m_s h^2 \end{bmatrix} \quad (15)$$

$$D_3 = \begin{bmatrix} 0 & m_s U & 0 \\ 0 & 0 & 0 \\ 0 & m_s h U & D_\phi \end{bmatrix} \quad (16)$$

The F and K matrices are unchanged, e.g.

$$K_3 = K_2, F_3 = F_2 \quad (17)$$

D. Model 4- 2DOF Model Assuming No Roll Dynamics

Finally, if one assumes that the sprung mass height is zero, the roll dynamics are completely eliminated because there is no longer any coupling from yaw or lateral velocity into roll. Without this coupling, there is no energy input to the roll model other than initial conditions. This assumption produces the well-known “bicycle model” which describes the vehicle’s planar dynamics [11].

$$M_4 = \begin{bmatrix} m & 0 & 0 \\ 0 & I_{zz} & 0 \\ 0 & 0 & 0 \end{bmatrix} \quad (18)$$

$$D_4 = \begin{bmatrix} 0 & mU & 0 \\ 0 & 0 & 0 \\ 0 & 0 & 0 \end{bmatrix} \quad (19)$$

$$K_4 = \begin{bmatrix} 0 & 0 & 0 \\ 0 & 0 & 0 \\ 0 & 0 & 0 \end{bmatrix} \quad (20)$$

Again, the F matrix is unchanged:

$$F_4 = F_3 \quad (21)$$

While this model does not include any roll dynamics and only exhibits lateral and yaw dynamics, it is included in this work because bicycle model parameters are used in all other models. It is therefore important to consider this model in

order to find or fit chassis parameters for models 1-3.

IV. OBTAINING VEHICLE INERTIAL PARAMETERS

To analyze validity of the models to describe vehicle chassis behavior, experiments were performed on a 5-door 1992 Mercury Tracer station wagon available at Penn State’s Pennsylvania Transportation Institute test track. A significant improvement over previous work is that this study was conducted using Novatel’s GPS/INS “SPAN” system. This GPS/INS system is based off two Novatel OEM4 dual frequency GPS receivers and the Honeywell HG1700 military tactical-grade IMU. This combination can provide estimates of position, velocity and attitude at rates up to 100Hz. In differential carrier phase fixed-integer mode and with continuous presence of GPS data, the system achieves a position solution with an accuracy of 2 cm. Attitude can be estimated with a 1-sigma accuracy of 0.013 degrees for roll, 0.04 deg for pitch and 0.04 degrees for yaw. All velocity errors are 0.007 m/s (one sigma) [12].

Many of the inertial parameters appearing in models 1-4 are easily measured or obtained from the National Highway Traffic Safety Administration database [13]. The table below presents these parameter values, units, and their source.

Variable	Value	Units	How obtained
m	1030	kg	Measured
m_s	824	kg	Estimated
W_f	6339	N	Measured
W_r	3781	N	Measured
l_f	0.93	m	NHTSA*
l_r	1.56	m	NHTSA*
L	2.49	m	Calculated
h	0.25	m	Measured
I_{zz}	1850	kg-m ²	NHTSA*
I_{yy}	1705	kg-m ²	NHTSA
I_{xx}	375	kg-m ²	NHTSA
I_{xz}	72	kg-m ²	NHTSA

*measurements were also made and these confirmed the NHTSA value to within a few percent

Estimates of sprung mass, m_s , were obtained by approximating the sprung mass as 0.8 times the total mass. The CG height was found to be 0.25 meters above the roll axis. The roll axis was found by video-taping the vehicle undergoing a rocking motion from the front and rear, determining the center of rotation at the front and rear axles, then using similar triangles to determine the axis of rotation at the center-of-gravity of the vehicle. Note that the sprung-mass height above the roll-axis is not the height of the CG above the road surface reported by NHTSA, 0.52 meters for this vehicle.

V. FITTING BICYCLE MODEL TIRE PARAMETERS

Several model parameters, especially the tire cornering stiffnesses, require experimental fitting and careful consideration of the tire’s impact on the model behavior. The models presented in this study lump right- and left-side

lateral tire forces to a single force on the front and rear axles, F_f and F_r . This single-wheel representation of a two-wheel axle is why the bicycle model is so named. Further, it is assumed that the lateral forces acting on each tire are directly proportional to the tire slip with proportionality constants on the front and rear tires of C_f and C_r respectively:

$$F_f = C_f \alpha_f, F_r = C_r \alpha_r, \quad (22)$$

The slip angles, α_i , are defined as the angle between the tire's orientation and the velocity vector of the center of the tire:

$$\alpha_f = \tan^{-1}\left(\frac{V + l_f \cdot r}{U}\right) - \delta_f \approx \frac{V + l_f \cdot r}{U} - \delta_f \quad (23)$$

$$\alpha_r = \tan^{-1}\left(\frac{V - l_r \cdot r}{U}\right) \approx \frac{V - l_r \cdot r}{U} \quad (24)$$

The simplifying assumptions made for Eqs. (23) and (24) are that the slip angles are small enough to allow a linear approximation and that right- and left-side differences in tire forces are negligible. With these assumptions, the tire forces can be written as:

$$F_f = C_f \left(\frac{V + l_f \cdot r}{U} - \delta_f \right) \quad (25)$$

$$F_r = C_r \left(\frac{V - l_r \cdot r}{U} \right) \quad (26)$$

Longitudinal forces acting upon the tires are assumed to be zero, and longitudinal velocity, U , is assumed to be constant.

The resulting expressions, when substituted into models 1-4 above, predict linear models. However, it is well known that the linearity assumption is violated under aggressive maneuvering. Others have noted that if the lateral acceleration remains below 0.4 g's, then assumptions of linearity appear to hold (many cite [14] as support). Therefore, care was taken in all testing to ensure that the experiments were conducted at lower accelerations.

To test whether or not linearity is actually preserved in the measured data, two frequency responses were conducted on the vehicle: one for steering inputs of small amplitude (1/4 rotation of the hand wheel) and one for large amplitudes (slightly less than 1/2 rotation of the handwheel). The resulting Bode plots are overlaid and shown in Figs. 1 and 2 below for the two states of the bicycle model, yaw rate and lateral velocity recorded at a speed of 25 mph. The linearity of the models is evident.

To find the cornering stiffnesses, two methods were used that are both based on steady-state data. Steady-state data was chosen since these data should be least influenced by model-to-model differences in high-order dynamics. The first fitting method attempts to match the DC gains of the sinusoidal frequency responses of Figs. 1 and 2. The second method is based on matching measured responses from steady-state turning around a skid-pad circle. Each is detailed below.

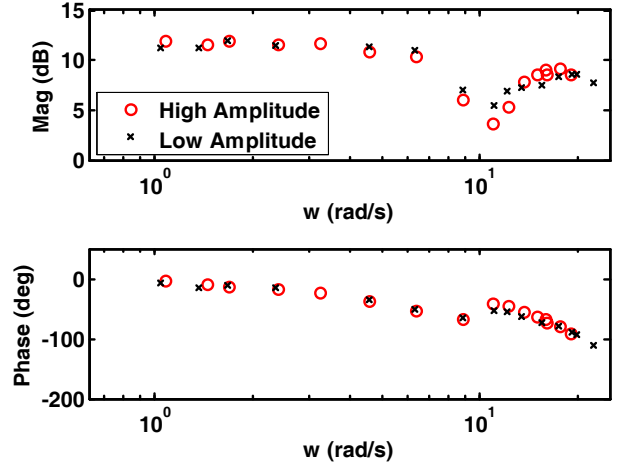


Figure 1: Frequency Response, Steering Input to Lateral Velocity

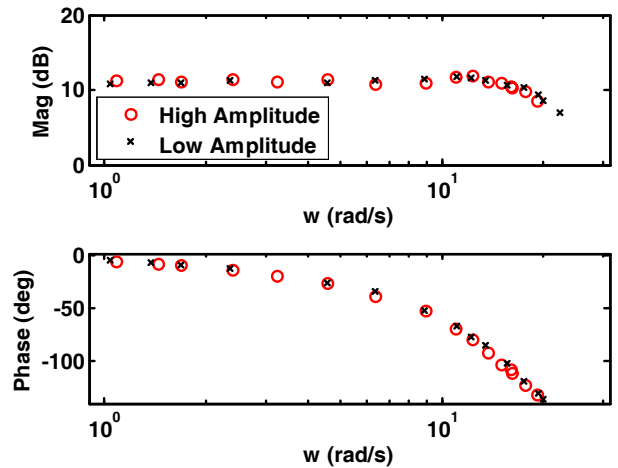


Figure 2: Frequency Response, Steering Input to Yaw Rate,

From the state-space form of Eq. (4), the DC gains, G , of the bicycle model from steering input to state output are given by:

$$G = D - CA^{-1}B \quad (28)$$

For lateral velocity, V , this DC gain was parametrically solved to be:

$$G_V = \frac{U \cdot ((C_f C_r) \cdot l_r \cdot L + C_f (l_f \cdot m \cdot U^2))}{C_f C_r \cdot (l_r^2 + l_f^2 + 2 \cdot l_f \cdot l_r) + m \cdot U^2 (C_f l_f - C_r \cdot l_r)} \quad (29)$$

and for yaw rate, r :

$$G_r = \frac{U \cdot (C_f C_r) \cdot L}{C_f C_r \cdot (l_r^2 + l_f^2 + 2 \cdot l_f \cdot l_r) + m \cdot U^2 (C_f \cdot l_f - C_r \cdot l_r)} \quad (30)$$

The numerical values of G_V and G_r can be read from Figs. 1 and 2 as 3.804 m/s lateral velocity per radian of steering input and 3.599 rad/sec yaw rate per radian of steering input,

Explore Litigation Insights

Docket Alarm provides insights to develop a more informed litigation strategy and the peace of mind of knowing you're on top of things.

Real-Time Litigation Alerts



Keep your litigation team up-to-date with **real-time alerts** and advanced team management tools built for the enterprise, all while greatly reducing PACER spend.

Our comprehensive service means we can handle Federal, State, and Administrative courts across the country.

Advanced Docket Research



With over 230 million records, Docket Alarm's cloud-native docket research platform finds what other services can't. Coverage includes Federal, State, plus PTAB, TTAB, ITC and NLRB decisions, all in one place.

Identify arguments that have been successful in the past with full text, pinpoint searching. Link to case law cited within any court document via Fastcase.

Analytics At Your Fingertips



Learn what happened the last time a particular judge, opposing counsel or company faced cases similar to yours.

Advanced out-of-the-box PTAB and TTAB analytics are always at your fingertips.

API

Docket Alarm offers a powerful API (application programming interface) to developers that want to integrate case filings into their apps.

LAW FIRMS

Build custom dashboards for your attorneys and clients with live data direct from the court.

Automate many repetitive legal tasks like conflict checks, document management, and marketing.

FINANCIAL INSTITUTIONS

Litigation and bankruptcy checks for companies and debtors.

E-DISCOVERY AND LEGAL VENDORS

Sync your system to PACER to automate legal marketing.